Synthetic access to a framework-stabilized and fully sulfided analogue of an Anderson polyoxometalate that is catalytically competent for reduction reactions

Jiaxin (Dawn) Duan,[†,#] Hafeera Shabbir,[ϕ,#] Zhihengyu Chen,[ǂ] Wentuan Bi,[†,§] Qin Liu,[†, §,*] Jingyi Sui,[†] Luka Đorđević,[†] Samuel I. Stupp,[†,∇,⊗] Karena Chapman,[ǂ] Alex B. F. Martinson,[‖] Alice Li,[†] Subhadip Goswami,[†] Rachel Getman[ϕ] and Joseph T. Hupp[†,*]

[§]School of Chemistry and Materials Science, University of Science and Technology of China, Hefei 230026, China

[†]Department of Chemistry, Northwestern University, Evanston, Illinois 60208, USA

[ϕ]Department of Chemical and Biomolecular Engineering, Clemson University SC

[‖]Materials Science Division, Argonne National Laboratory, 9700 South Cass Avenue, Argonne, Illinois 60439, United States

[ǂ]Department of Chemistry, Stony Brook University, New York 11794-3400, USA

[∇]Department of Biomedical Engineering and Department of Materials Science and Engineering, Northwestern University, Evanston, Illinois 60208, United States

[⊗]Simpson Querrey Institute for BioNanotechnology and Department of Medicine, Northwestern University, Chicago, Illinois 60611, United States

X-ray Absorption Spectroscopy, Pair distribution function analysis (PDF), Difference envelope density (DED), Isolated Metal-sulfide Clusters, Metal-Organic Frameworks, Hydrogen evolution reaction, Density Functional Theory

ABSTRACT: Polyoxometalates (POMs) featuring 7, 12, 18, or more, redox-accessible transition-metal ions are ubiquitous as selective catalysts, electrocatalysts, and sensitized photocatalysts, especially for oxidation reactions. The corresponding synthetic and catalytic chemistry of stable, discrete, and capping-ligand-free poly***thio***metalates (PTMs), which could be especially attractive for reduction reactions, is much less well developed. Among the challenges is the propensity of PTMs to agglomerate and form larger clusters of indeterminate size, as well as the tendency for agglomeration to block access of candidate reactants to potential catalyst active-sites. Nevertheless, the pervasive presence of transition-metal sulfur clusters metalloenzymes or cofactors that catalyze reduction reactions, and the justifiable proliferation of studies of 2D metal-chalcogenides, and especially their edge sites, as reduction catalysts, point to the promise of well-defined and controllable PTMs as catalysts for reduction reactions, including complex, bond-forming, many-electron reactions. Here we report the fabrication of agglomeration-immune, reactant-accessible, capping-ligand-free $Co^{II}Mo^{IV}_6S_{24}{}^{n-}$ clusters as periodic arrays in a water-stable, hierarchically porous Zr-metal-organic-framework (MOF; NU1K) by first preparing and installing a disk-like Anderson polyoxometalate, $Co^{II}Mo^{VI}_6O_{24}{}^{m-}$, in size-matched (<1 nm) micropores termed *c*-pores, where the siting is established via DED (difference electron density) X-ray diffraction experiments. Prolonged treatment with flowing H_2S while heating, uniformly reduces the six molybdenum(VI) ions to Mo(IV) and quantitatively replaces oxygen anions with similarly ligating sulfur anions in the form S^{2-}, HS^-, and $S_2{}^{2-}$. Further DED measurements show that the templated POM-to-PTM conversion leaves the clusters individually isolated in open-channel-connected *c*-pores. The structure of the immobilized cluster as determined, in part, by XPS, XAFS, and PDF (pair-distribution function) analysis of total X-ray scattering agrees very well with the theoretically simulated structure. Preliminary, proof-of-concept experiments show that electrode-supported thin-films of $CoMo_6S_{24}$@NU1K are electrocatalytically competent for hydrogen evolution in aqueous acid (*e.g.* 10 mA·cm^{-2} of current density at an overpotential of 100 mV). Suspensions of $CoMo_6S_{24}$@NU1K in acetonitrile + triethanolamine, are photocatalytically competent for hydrogen evolution via sensitization with chromophoric MOF linkers. Nevertheless, the initially installed PTM appears to be a pre-catalyst, as hydrogen evolution is observed only after four hours of photolysis. Reduction-assisted loss of ~3-to-6 sulfurs, as H_2S, likely is responsible for pre-catalyst-to-catalyst conversion, as the loss opens coordination sites on multiple cluster-sited metal ions, perhaps enabling hydrogen evolution via a Mo-hydride intermediate. Given the great variety of sizes and compositions available for both POMs and Zr-MOFs, we suggest that the approach described here can be adapted for the synthesis and stabilization of periodic arrays of other non-agglomerating, capping-ligand-free PTMs of well-defined metal-nuclearity, presumably including catalytically functional PTMs.

INTRODUCTION

By using enzymes, metal-containing cofactors, and related species, Nature has catalytically optimized selectivities and rates of numerous reduction and oxidation reactions, including reactions essential for sustaining life. Metal-oxygen adducts are known to catalyze selective oxidation reactions. The manganese/calcium-oxo cubane in the oxygen evolving complex in Photosystem II is an example, as is cytochrome P450 for catalysis of oxidative metabolism.[1-3] For reduction and electron transport, Nature often uses enzyme co-factors that contain pairs or clusters of first-row transition metal ions coordinated, in part, by sulfur. Examples are Fe-Fe- and Fe-Ni-containing hydrogenases,[4,5] molybdenum-iron (+sulfur),[6] vanadium-iron (+sulfur),[7] and all-iron (+sulfur) containing nitrogenases,[8] and iron-sulfur cubanes for electron transport.[9] Taking inspiration from Nature we want to explore stabilized, cluster-based metal-chalcogenide catalysts for reductive chemical transformations.

Synthetic metal-oxide films, nanoparticles, clusters, etc. are excellent for catalyzing, electro-catalyzing, and/or photo-catalyzing oxidation reactions. Of these compounds, polyoxometalates (POMs) are of particular interest to us. They are a special class of metal (*e.g.*, V^{V}, Mo^{V}, Nb^{V}, Ta^{V}, Mo^{VI}, and W^{VI}) oxide polyanion clusters bridged by oxygen atoms that form well-defined cluster frameworks with adjustable structures and tunable compositions.[10,11] An enormous variety of well-characterized polyoxometalates exists and many of these can catalyze oxidation reactions, but, they often fall short as catalysts for reduction reactions. [12-16]

In principle, one-to-one sulfur-for-oxygen analogues of POMs, *i.e.* poly*thio*metalates (PTMs), ought to be synthetically accessible. In practice, the literature is sparse if one ventures beyond tetranuclear transition-metal complexes into the realm of Anderson (seven metal ions), Keggin (twelve metal ions), Dawson (eighteen metal ions) or larger and similarly well-defined, clusters. Nevertheless, synthetic access to capping-ligand-free, sulfur-based analogues of POMs could open-up new reductive catalytic chemistry.

We suggest that the paucity of PTMs is due to challenges in stabilizing clusters against agglomeration, without resorting to capping-ligands which can block catalyst active-sites. We recently reported that Mo(VI)/Rh(III)-based, Anderson-type poly*oxo*metalates can be controllably heterogenized, protected against sintering, even at 200°C, and employed catalytically for a representative, gas-phase oxidation reaction, under thermally demanding conditions.[17] Our approach was to site the POMs within size-matched pores of a hierarchically porous, metal-organic framework (MOF) such that periodic arrays of reactant-accessible, yet immobile, clusters are presented. Related work has been described for Keggin POMs, with the organized POMs then being deployed as heterogeneous catalysts for condensed-phase oxidation reactions.[18,19] We reasoned that similarly useful arrays of agglomeration-immune PTMs could be obtained by starting with pre-isolated POMs. The obtained arrays could then be deployed as heterogeneous catalysts for reduction reactions.

Here we report that uniformly organized arrays of non-aggregating polythiometalates can indeed be accessed by subjecting spatially separated, MOF-immobilized, reactant-accessible POMs to heating under H_2S. We also report that the arrays exhibit salutary reductive catalytic activity for an intentionally simple, model reaction.

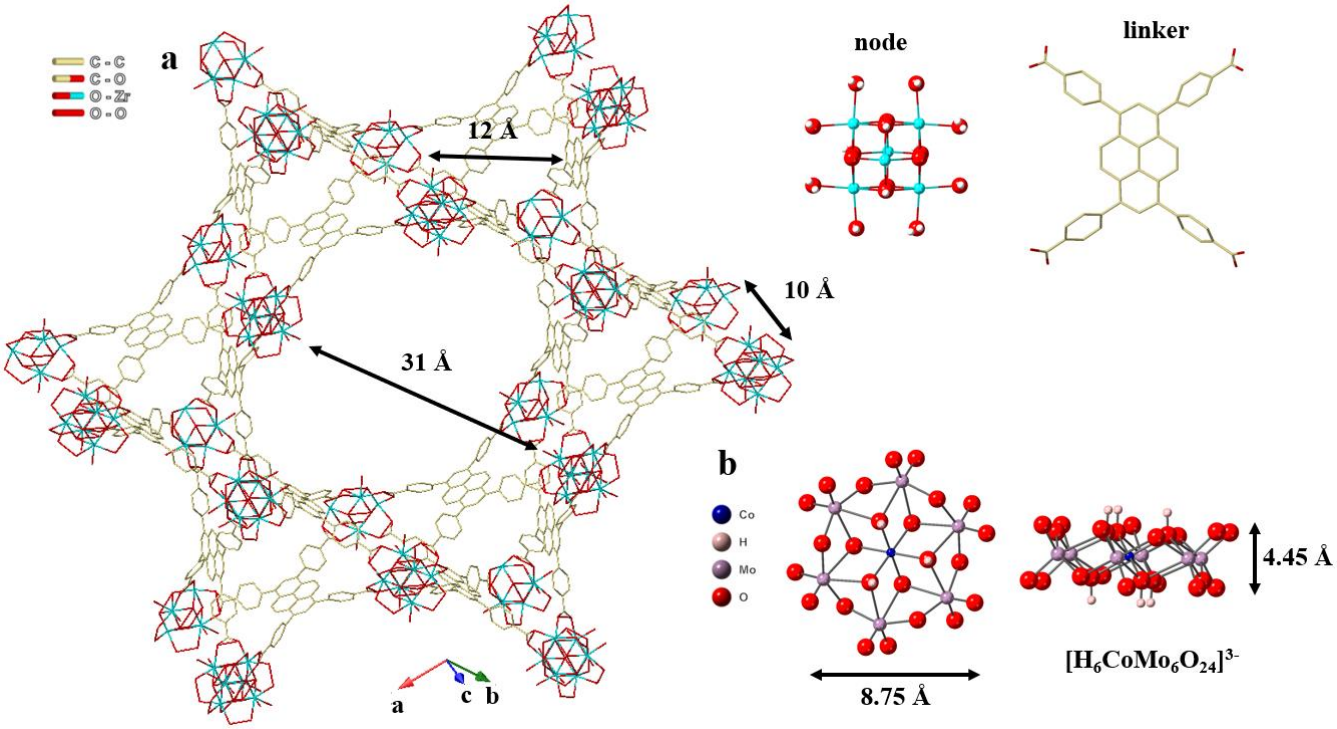

Figure 1. (a) Crystal structure of NU1K, showing the 31 and 12 Å channels. Each layer is separated by 10 Å windows. The structures for the nodes and linkers are given. Polyhedral representation and size of (b) $[H_6CoMo_6O_{24}]^{3-}$ seen from a top view and a side view.

RESULTS AND DISCUSSION.

Synthesis. As a cluster-catalyst support, we selected the metal organic framework NU1K (NU-1000; Figure 1a).[20] (Recall that MOFs, including NU1K, are extended porous solids; only a tiny, illustrative portion is shown.) Like many MOFs, NU1K displays a sizable internal surface array: ~2,200 m^2g^{-1} – roughly twice that of the highest area zeolite and comparable to many high-area porous carbon formulations. As a broad class, MOFs offer regularity/periodicity of void spaces, tunability of pore sizes, and adjustability of pore surface (interior surface) properties.[21] Zr-MOFs, including NU1K, have been shown to be stable under a wide range of thermal and chemical conditions.[22] NU1K ideally is composed of $Zr_6(\mu_3\text{-}O)_4(\mu_3\text{-}OH)_4(H_2O)_4(OH)_4$ nodes and tetratopic 1,3,6,8-(p-benzoate)pyrene ($TBAPy^{4-}$) linkers.[23] However, depending on the specifics of its activation (*i.e.*, removal of synthesis solvent and growth modulators), up to 75% of the nonstructural aqua + hydroxo node-ligand pairs may be adventitiously displaced by bridging formate anions. The activation procedure used (see Supplemental Information) leaves the material with multiple formate ligands per node.[24,25] Independent of formate content, NU1K offers 1D hexagonal and triangular channels of diameters ~31 Å and ~12 Å, respectively, as well as cross-connecting pores (termed c-pores) of just under 10 Å diameter (Figure 1a).[20,25,26]

Having previously studied in detail the installation, siting, and resistance to migration of the Anderson POM, $RhMo_6O_{24}^{n-}$,[17] we started with a closely similar POM, $(NH_4)_3[H_6CoMo_6O_{24}]\cdot 7H_2O$ (denoted as $CoMo_6O_{24}$) (Figure S1). This POM comprises a $\{CoO_6\}$ octahedron connected to six $\{MoO_6\}$ octahedra in an edge-sharing mode, to form a planar, disk-like cluster (Figure 1b).[27] The dimensions of $CoMo_6O_{24}$ are approximately 8.55 Å × 8.55 Å × 3.15 Å, which fit well within the *c*-pore of NU1K. We successfully encapsulated $CoMo_6O_{24}$ via impregnation from aqueous solution; the resulting hybrid material we refer to as $CoMo_6O_{24}$@NU1K.

In prior works,[28,29] we found that hydrothermal processes that incorporate organic sulfur into Mo_7 can be efficient for obtaining highly purified and stable metallic 1T-MoS_2 With the hypothesis that Anderson type POMs have the structural potential to yield discrete, cluster-sized analogues of bulk 1T-MoS_2 and the knowledge that NU1K itself, is refractory toward H_2S, even at elevated temperature,[30,31] we attempted the synthesis of isolated , c-pore-confined $CoMo_6S_{24}$ clusters from H_2S and $CoMo_6O_{24}$@NU1K. We found, after experimental optimization, that heating in a tube furnace at 180 °C under flowing H_2S for 24h accomplishes quantitative conversion; see Supplemental Information. *Caution: Inhalation of H_2S can be deadly; its handling, delivery, and removal must be carefully managed.* Here, H_2S functions not only as a source of sulfur, but also as a reductant for converting Mo(VI) primarily to Mo(IV), while the POM serves as a spatially isolated template for the PTM.

For comparison, bulk $CoMo_6S_x$ was prepared under similar conditions but with higher reaction temperature using bare $CoMo_6O_{24}$ without NU1K (Figure S6-8). Also prepared for comparison were Mo_7O_{24}@NU1K and MoS_x@NU1K; see Supplementary Information.[17]

Characterization. $CoMo_6O_{24}$@NU1K and $CoMo_6S_{24}$@NU1K unit cells, as seen by the Bragg peak positions on powder X-ray diffraction (Figure 2a), resemble that of NU1K, except for a decrease in the intensity of diffraction peaks at 2θ=7.44° corresponding to a decrease in the coherency of planes with a spacing of 1.0 nm (highlighted in yellow in

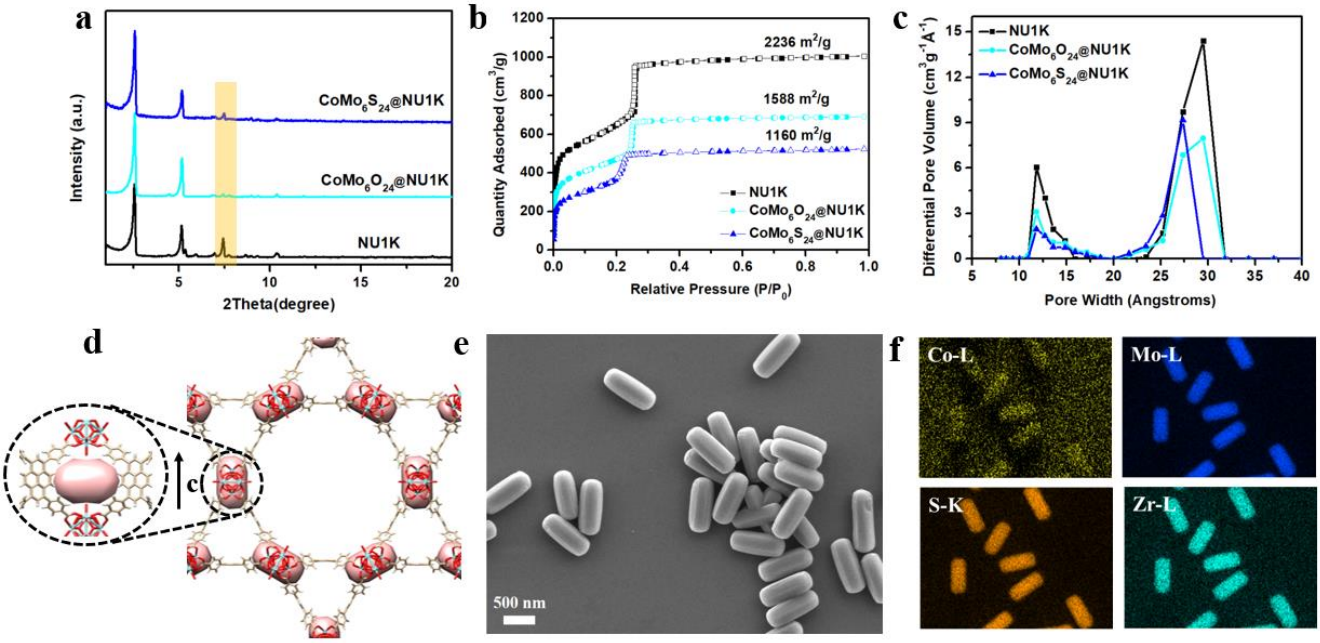

Figure 2. (a) PXRD patterns (b) and (c) are N_2 isotherm and pore size distribution of NU1K, $CoMo_6O_{24}$@NU1K and $CoMo_6S_{24}$@NU1K. DEDs corresponding to the location of (d) $CoMo_6S_{24}$@NU1K (pink surface) in electron density viewed parallel to the c-axis. (e) SEM and (f) EDS mapping of NU1K after $CoMo_6S_{24}$ incorporation, indicating the homogeneous distribution of cobalt, molybdenum, sulfur, and zirconium.

Figure 2a). The diffraction pattern matches well with a predicted/simulated pattern where the POM is located between two nodes in inter-channel windows (*c*-pores).[18]

BET surface areas calculated from N_2 isotherms of $CoMo_6O_{24}$@NU1K (1588 m^2/g) and $CoMo_6S_{24}$@NU1K (1160 m^2/g) are significantly smaller than that of bare NU1K (2236 m^2/g; Figure 2b). In part, the decreases reflect increases in sample mass. The cluster@NU1K isotherms show a type IV feature, similar to that of NU1K, which is associated with the filling of mesopores. Isotherm-derived pore size distributions (PSDs) indicate for both samples contraction of mesopore and micropore widths (Figure 2c) – a phenomenon that has been associated elsewhere with displacement or elimination of node-ligated formate ions when followed by thermal activation.[25] More striking are the large decreases in the volume of the triangular micropores, an indication that the *c*-pore-sited clusters extend into the triangular channels/pores. The decrease with $CoMo_6S_{24}$@NU1K is greater than with $CoMo_6O_{24}$@NU1K, of S relative to O.

For a more direct assessment of PTM and POM siting, we turned to difference envelope density (DED) analysis of synchrotron-based X-ray scattering data.[32] The analysis shows that the disk-like clusters are centered in the *c*-pore of NU1K, but extend into the triangular micropores; see Figures 2d and S2.[33] SEM images show that the size and morphology of NU1K crystallites are well maintained after H_2S annealing (Figure 2e) with no obvious presence of nanoparticles or clusters on exterior surfaces. EDS mapping suggests that Co, Mo and S are evenly distributed throughout the MOF. Co, Mo and S spatial distributions match well with that of Zr (Figure 2f), suggesting uniform dispersion of isolated $CoMo_6S_{24}$ cluster throughout the crystal, rather than their accumulation at regions near the crystal surface. $CoMo_6O_{24}$ clusters are also uniformly distributed within NU1K; see Figure S3.

For $CoMo_6O_{24}$@NU1K, after 125°C heating in Ar overnight to remove physisorbed water, the sharp band of NU1K, peaking at ~3750 cm^{-1} and associated with an O-H stretch for μ_3-hydroxo ligands, is replaced with a broad band maximizing at 3667 cm^{-1} for $CoMo_6O_{24}$@NU1K, while the formate-associated band at 2745 cm^{-1} disappears (Figure 3a).[25] Thus, we infer that formate anions are displaced by POM anions. The protons of the four μ_3-hydroxos are the most acidic of the sixteen protons ideally offered by each ligated node.[34] Their loss, as implied by the disappearance of the IR peak at 3750 cm^{-1}, suggests Bronsted acid/base or other interactions with the installed POMs.

ICP-OES yields a Co:Mo molar ratio of 1:6, consistent with the chemical composition of $CoMo_6O_{24}$. Approximately 0.87 POM per Zr_6 node is the maximum loading in NU1K after thorough washing. After H_2S annealing, the molar ratio of Co to Mo remains 1:6, while S:Mo is 3.87:1. The loading and elemental ratios for the putative $CoMo_6S_{24}^{m-}$ PTM in NU1K are nearly identical to those of the $CoMo_6O_{24}^{n-}$ template, implying that sulfur completely replaces oxygen during H_2S annealing.

The chemical composition of the synthesized $CoMo_6S_{24}$@NU1K was further interrogated via X-ray photoelectron spectroscopy (XPS). The Mo 3d spectrum consists of peaks located at approximately 228.7 and 231.8 eV, which correspond to the $3d_{5/2}$ and $3d_{3/2}$ components, respectively, of Mo^{4+} in $CoMo_6S_{24}$@NU1K (Figure 3b). A broad S 2s feature was observed near the Mo $3d_{5/2}$ peak, which indicates multiple chemical states of sulfur. For further analysis, we examined the S 2p region, which was

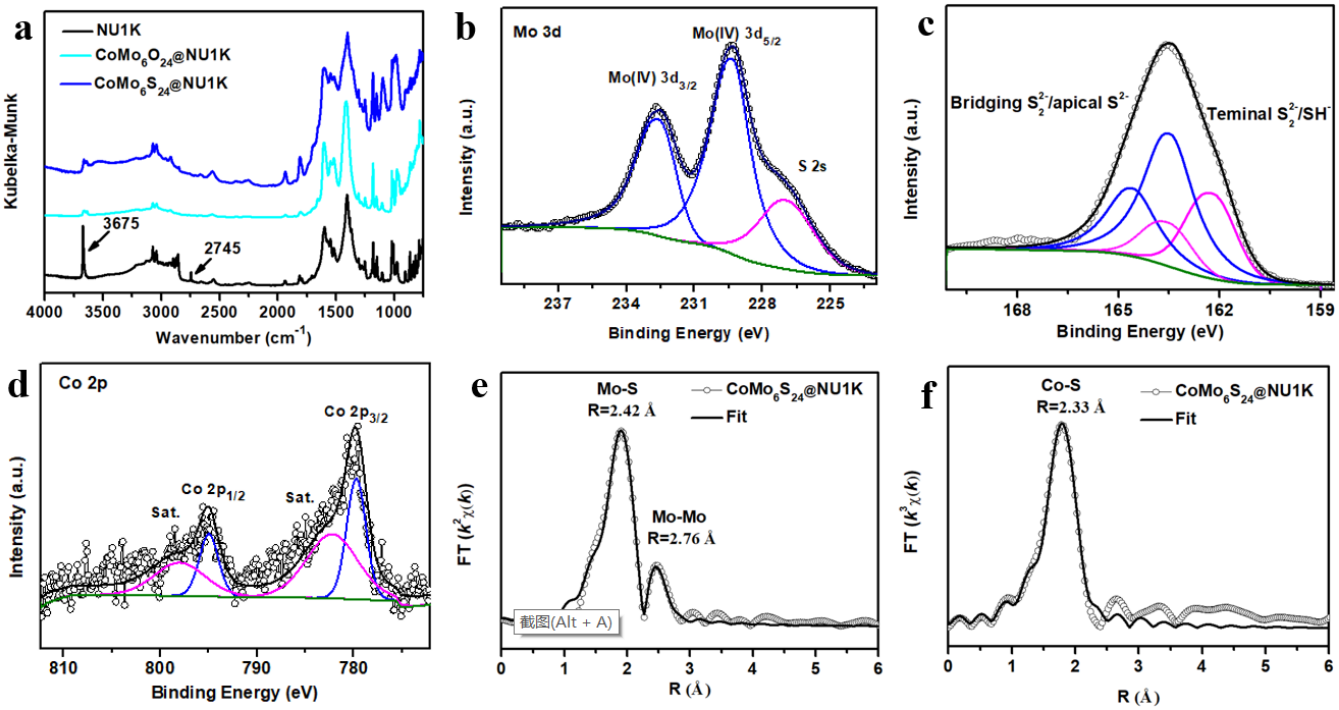

Figure 3. (a) DRIFT spectra of the NU1K, $CoMo_6O_{24}$@NU1K and $CoMo_6S_{24}$@NU1K. Vibrational spectra recorded at 125 °C overnight in Argon. XPS spectra showing Mo 3d (b), S 2p (c) and Co 2p (d) core-level peak regions of $CoMo_6S_{24}$@NU1K. (e) Fitting curves for EXAFS data at the Mo K-edge for $CoMo_6S_{24}$@NU1K. (f) Fitting curves for EXAFS data at the Co K-edge for $CoMo_6S_{24}$@NU1K.

fitted with two distinct doublets ($2p_{3/2}$, $2p_{1/2}$) (Figure 3c): (1) one doublet at (162.3 eV, 163.5 eV), which arises from terminal SH^- and S_2^{2-} ligands, (2) one doublet at (163.6 eV, 164.8 eV), which reflects the presence of bridging S_2^{2-} and apical S^{2-} ligands.[29] The convolution of Co 2p XPS spectra features is displayed in Figure 3d. A prominent pair of peaks at around 779.78 and 795.00 eV can be attributed to Co(II) $2p_{3/2}$ and $2p_{1/2}$, respectively. Satellite shake-up peaks at 782.27 eV and 798.13 eV in the spectrum of the as-prepared catalyst confirm the presence of cobalt in oxidation state II.[35]

Synchrotron-based X-ray absorption spectroscopy (XAS) was used to characterize the local structure of $CoMo_6S_{24}$@NU1K. FT curves at the Mo K-edge (Figure 3e) are characterized by two main peaks at 2.42 Å and 2.76 Å, corresponding to the nearest Mo-S and Mo-Mo bonds. Quantitative FEFF fitting establishes the similarity of Mo local structure in $CoMo_6S_{24}$@NU1K to that found in 1T'-MoS_2. Indeed, within the uncertainties of published crystal structures of 1T'-MoS_2, XAS-derived bond lengths for the MOF-enshrouded PTM cluster agree with the former (Supplementary Table 1). To assess the local chemical environment of the lone cobalt center, the XAS spectrum at the Co K-edge was measured. Quantitative fitting of the EXAFS spectrum (Figure 3f) reveals that the local structure of Co is similar to that of Mo, with a fitted Mo-S bond length of 2.42 Å in the Mo K-edge and Co-S bond length of 2.33 Å in the Co K-edge and, fitted Mo-S and Co-S coordination numbers of 6. These results together point to retention of Co, and little structural disruption in the molybdenum-rich host cluster following sulfidation (trans-chalcogenation). The corresponding FT curves are fitted via the ARTEMIS model to obtain the quantitative parameters of the local structure near the element Mo and Co. Fitting results are summarized in Supplementary Table 1.[29]

The pair distribution function (PDF) provides a histogram of all atom-atom distances within the material, weighted by their scattering power. The differential PDF (dPDF) obtained by subtracting the PDF for NU1K from that obtained of $CoMo_6O_{24}$@NU1K and $CoMo_6S_{24}$@NU1K, isolates the contribution from the guest cluster and its interaction with the MOF. The dPDF of $CoMo_6O_{24}$@NU1K is well fit by a structural model derived from the $CoMo_6O_{24}$ structure (Figure S4a). The a, b and c in the Figure S4a correspond to the different Mo···Co/Mo distances of 3.3 Å, 5.7 Å and 6.6 Å of Figure S4b. Table S2 shows the one-to-one correspondence between the atomic pairs assigned to all peak positions in the PDF and that of the crystal structure. There is a slight shift of peaks in the experimental dPDF compared to the simulated model, which could potentially be associated with a distortion or relaxation of the cluster when confined in the *c*-pore. By comparison, the $CoMo_6S_{24}$ cluster is more disordered, with only a few well-defined peaks discernable at low *r*. From Figure 4a, peaks at 2.42 Å, 2.75 Å and 3.36 Å are attributed to the nearest Co/Mo-S, the nearest Mo-Mo, and Mo--Mo pairs, respectively. Among these, the nearest Co/Mo-S, the nearest Mo-Mo bond lengths match well with above EXAFS fitting results.

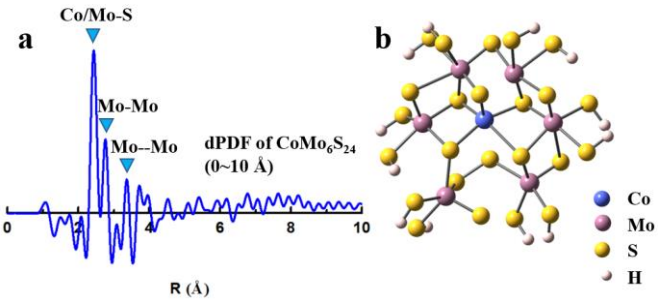

Figure 4. (a) $CoMo_6S_{24}$@NU1K obtained by subtraction of the PDF for pristine NU1K. (b) Simulated structure best matching (a) experimental bond from dPDF.

Density functional theory (DFT) simulations were also carried out to provide molecular level insights into the structure. As fully sulfided analogues of the Anderson POM are unknown, we started from the structure of Mo_7O_{24} (Figure S5) and replaced the central Mo atom with a Co atom and all O atoms with S atoms. We then varied the H and S contents, chemical states of S, and overall cluster charges and performed geometry relaxations in DFT. The structural model of the cluster was evaluated by comparing the dPDF, S:Mo ratios, Mo coordination numbers and Mo oxidation states of all experimental data with computed models. The calculated structures that give the best agreement with experiment are negatively charged. The structure that agrees best with experimental dPDF results comprises terminal SH^-, bridging and terminal S^{2-}, and bridging S_2^{2-} ligands (Figure 4b). Thus, the arrangement and configuration of the main-group element in the PTM is richer than in the parent POM. Notably, this unique cluster exposes a large fraction of sulfur atoms as edge-sited atoms

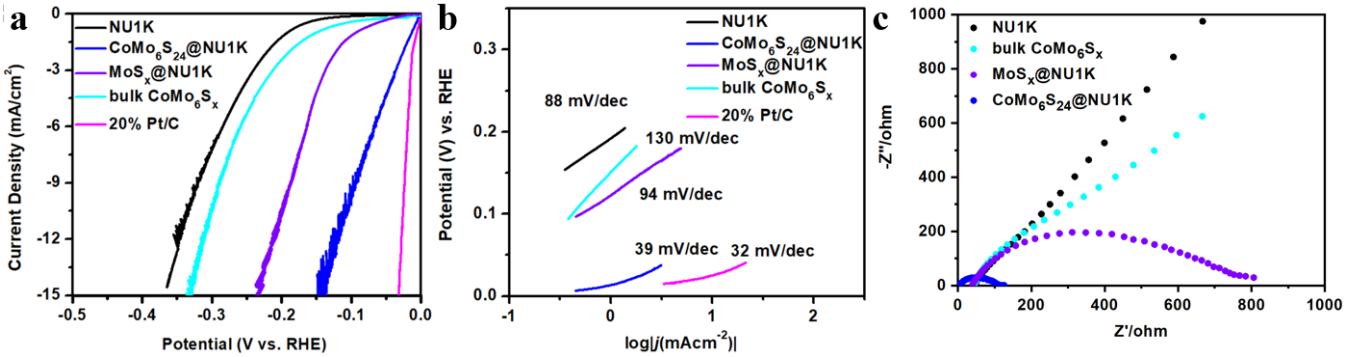

Figure 5. HER catalytic performances for $CoMo_6S_{24}$@NU1K. (a) Polarization curve of all catalysts in 0.5 M H_2SO_4 (scan rate: 2 mV s^{-1} under a three-electrode configuration). (b) Tafel plots. (c) Electrochemical impedance spectroscopy (EIS) of $CoMo_6S_{24}$@NU1K.

– a point of direct relevance for envisioned catalytic applications.

Electrocatalysis. For simplicity, we selected the hydrogen evolution reaction (HER) as a probe reaction for gauging the catalytic efficacy of $CoMo_6S_{24}$@NU1K. HER polarization curves for various electrode-supported, lab-prepared samples (see Supplementary Information for details) and commercial Pt/C in 0.5 M H_2SO_4 are shown in Figure 5a. As expected, 20% Pt/C exhibits the highest HER electrocatalytic activity with near-zero onset potential. To investigate the efficacy of $CoMo_6S_{24}$@NU1K for HER activity, control experiments of bulk $CoMo_6S_x$, MoS_x@NU1K and NU1K were performed under the same conditions. The overpotentials of bulk $CoMo_6S_x$, MoSx@NU1K and NU1K are 300, 195, and 330 mV, respectively, when the cathodic current-density reaches 10 mA·cm^{-2}. $CoMo_6S_{24}$@NU1K is highly active toward HER, demonstrated by a rapid rise in cathodic current density to 10 mA·cm^{-2} at -100 mV vs RHE. More importantly, $CoMo_6S_{24}$@NU1K in acidic medium shows better current density (10 mA·cm^{-2}) at the overpotential of 100 mV vs. RHE than most MoS_2 electrocatalysts reported to date, including Co-doped two-dimensional MoS_2,[36] Co-doped edge sites in vertically aligned MoS_2,[37] MoS_2 Basal Plane S-Vacancy by Co cluster addition,[38] Co-MoS_2,[39] UiO-66-NH_2-MoS_2,[40] NU-1000-Ni-S,[30] and NU-1000-MoS_x-SIM.[31]

While mechanistic studies are beyond the scope of this work, Tafel slopes can, in favorable cases, provide mechanistic insight;[41] see Figure 5b. For 20% Pt on carbon, a champion material for HER, the slope is 32 mV dec^{-1}. For $CoMo_6S_{24}$@NU1K, the Tafel slope varies from ~32 mV·dec^{-1} at low overpotential to 120 mV·dec^{-1} at comparatively high overpotential. Bulk $CoMo_6S_x$, MoS_x@NU1K, and NU1K yield Tafel slopes in the range of *ca.* 90 to 130 mV dec^{-1}. In cases where catalyst coverage by adsorbed hydrogen atoms (H*) is modest, and not strongly potential dependent, Tafel slopes in this range typically indicate a rate-limiting Volmer initial step: $H^+ + e^- + * \rightarrow H^*$, where "*" signifies an adsorption site. A Tafel slope near 30 mV·dec^{-1} typically points to fast Volmer steps, followed by a rate-limiting Tafel step: $2H^* + 2* + H_2$. A Tafel slope near 40 mV·dec^{-1} typically points to a fast Volmer step, followed by a rate-limiting Heyrovsky step: $H^* + H^+ + e^- \rightarrow H_2 + *$.[41] The mechanism for HER at Pt in aqueous acid is generally believed to be the Tafel-Volmer mechanism.

The simplest interpretation of a curved Tafel plot for $CoMo_6S_{24}$@NU1K is that the mechanism for HER, or at least the rate-determining step, changes as function of electrochemical driving force. A more prosaic interpretation is that $CoMo_6S_{24}$@NU1K is poorly conductive, and that the potential-dependence of the HER rate (current) is dominated by the ohmic resistance of the catalyst itself. Note that instrument-based iR corrections cannot compensate for catalyst resistance. Follow-up studies will be needed in order to gauge the importance of this effect. The observed Tafel slope at low overpotential is suggestive of a Volmer-Tafel mechanism where two electrons are transferred before rate-limiting chemical reactivity between pairs of sorbed H atoms, presumably sited on catalyst sulfur ions. An intriguing and speculative alternative, however, is rapid transfer of a pair of electrons to a proton to yield a Mo^{IV}-hydride, followed by rate-determining H_2 formation from the hydride and a sulfide-sited proton. We have shown elsewhere that when single $Mo(SH)_2$ units are grafted to the hexa-zirconium(IV) node of NU1K via Mo-O-Zr and Mo-(OH)-Zr linkages, yielding Mo(IV) in a distorted tetrahedral environment, electrocatalytic hydrogen evolution occurs via Mo(IV) reduction to Mo(II) followed proton recruitment to form Mo^{IV}-hydride, and rate-determining reaction of the hydride with a sulfur-sorbed proton.[31] Thus, in the single-metal-ion limit, the molybdenum-sulfur catalyst generates H_2 via a mechanism reminiscent of the behavior of various hydrogenases. For the mechanism to be viable with a PTM, loss of a sulfide, sulfhydryl, or disulfide ligand, and exposure of a molybdenum site would be required. While further studies will be needed to gauge catalyst evolution and pin-down the HER mechanism, preliminary computational studies support the notion of labialization of sulfur species upon reduction of molybdenum.

The apparent superiority of $CoMo_6S_{24}$@NU1K as an HER catalyst was corroborated by electrochemical impedance spectroscopy (EIS) measurements at -35 mV vs. RHE. As shown in Figure 5c for $CoMo_6S_{24}$@NU1K, a Nyquist plot yields a single semicircle. From the semicircle we obtain a charge-transfer resistance (R_{ct}) of 100 Ω. Notably, R_{ct} is much larger (and hydrogen evolution is much slower) for bulk $CoMo_6S_x$, MoSx@NU1K and NU1K catalysts – consistent with voltammetry results in Figure 5a and Tafel plots in 5b.

The basis for the superior performance of $CoMo_6S_{24}$@NU1K relative to bulk $CoMo_6S_x$ almost certainly includes the much higher areal density of the former. A close-packed monolayer of flat Anderson-type PTMs on a flat electrode amounts to about 6 x 10^{-10} mol/cm^2 – perhaps a reasonable lower limit estimate of the number of exposed active-sites for a nonporous, film-like monolith of bulk $CoMo_6S_x$, For $CoMo_6S_{24}$@NU1K the real density PTM units is 500× higher, when loaded as described in the Supplemental Information. It seems likely that the redox conductivity of $CoMo_6S_{24}$@NU1K is insufficient to enable active-sites far from the PTM@MOF/electrode interface to participate electrocatalytically to the extent that those close to the interface participate. Even semi-quantitative assessment will require charge-transport studies that are beyond the scope of this initial paper. Nevertheless, if we take 500-fold as an upper limit for the increase in fully participating electrocatalytic active-sites for electrode-immobilized $CoMo_6S_{24}$@NU1K relative to electrode-immobilized, bulk $CoMo_6S_x$, and if we assume a Tafel slope of 120 mV·dec^{-1}, the loading difference translates to a decrease in HER overpotential of ~320 mV at current densities of 10 mA cm^{-1}. An arguably more realistic ratio of fully addressable HER active-sites for electrode-immobilized $CoMo_6S_{24}$@NU1K versus electrode-immobilized, bulk $CoMo_6S_x$, is 20. This catalyst areal loading capacity translates to a decrease in HER overpotential of 156 mV. Regardless, the high areal-concentration of PTM-based active-sites appears, on its own, to confer a substantial decrease in HER kinetic overpotential. *This observation underscores a key potential advantage of presenting active-sites via MOF-installation, compared with simply immobilizing the same catalyst on a flat electrode at monolayer density.* No doubt, other factors are important, but their assessment will require much more

detailed kinetics studies. Finally, it may be useful to frame electrocatalytic activity in terms of local turnover-frequency (TOF). If, for simplicity, we assume one active-site per PTM in a $CoMo_6S_{24}$@NU1K coating and a kinetically effective loading equivalent to 500 monolayers of reactant-accessible PTM, we obtain a TOF ~1 s^{-1} at an iR-corrected overpotential 100 mV. If the electrocatalytically effective areal concentration is equivalent to, say, 20 monolayers of PTM, the effective TOF for the small fraction of sites actively participating, would be ~25 s^{-1}.

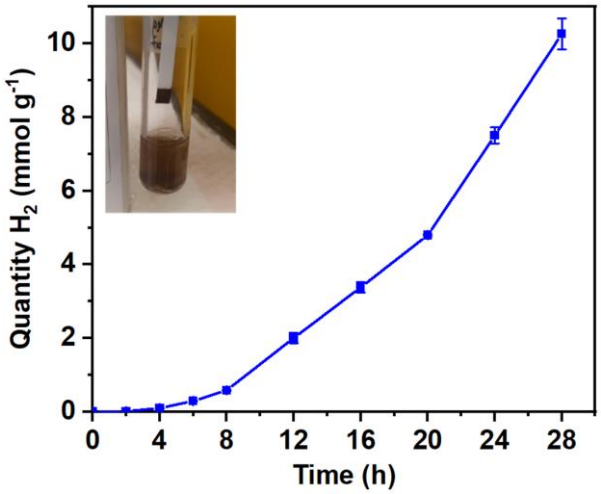

Figure 6. Photocatalytic hydrogen evolution by $CoMo_6S_{24}$@NU1K. Inset figure shows the change in color of the paper strip during first 4 h of the reaction due to H_2S evolution.

Photocatalysis. Previously, we have shown that NU1K can act as a light-harvesting antenna to transfer redox equivalents to node-anchored redox quenchers and redox-catalysts.[42,43] We reasoned that similar behavior might be seen here. We then qualitatively evaluated suspensions of $CoMo_6S_{24}$@NU1K as photocatalysts for hydrogen evolution. To regenerate the light-absorbing tetraphenyl-pyrene linker following electron-transfer to a PTM-based catalyst we employed a sacrificial electron donor, triethanolamine (TEOA). For these preliminary experiments we relied upon residual water in the solvent acetonitrile as a proton source, while recognizing that TEOA might also function as a proton source. We irradiated $CoMo_6S_{24}$@NU1K suspensions with the reaction mixture at 390 nm light, and recorded H_2 evolution for 30 h. As shown in Figure 6, 10 mmol of H_2 were obtained per gram of contained $CoMo_6S_{24}$ catalyst. Assuming, for simplicity, one active-site pair per PTM, this amount translates to ~28 catalytic turnovers.

The most intriguing feature of the plot in Figure 6 is the *ca.* 4h induction period before H_2 is detected – behavior that is often linked with catalyst evolution toward a more potent form. Following closed-cell sample irradiation, the opened photochemical cell emitted an H_2S-like odor. Qualitative assessment of the solution in the cell using a commercial silver-containing test strip yielded a change in strip color from white to dark brown, consistent with silver sulfide formation. XPS examination of the darkened test strip confirmed the presence of S^{2-}, but neither cobalt nor zirconium. Finally, post-catalysis assessment of PTM@MOF composition revealed losses of between 3.5 and 6 sulfide ions from the *ca.* 24 initially present. The combined results point to sulfide loss as a key step in converting $CoMo_6S_{24}$@NU1K from catalytically inactive to catalytically active form.

For bulk MoS_2, introduction of S-vacancies is known to enhance (electro)catalytic activity for HER,[44] where the basis for enhancement appears to be lattice strain that, in turn, translates to stronger affinity of sulfide sites for H atoms. While a similar effect conceivably could be operative here, an attractive, albeit speculative, alternative explanation is that exposure of initially octahedral molybdenum ions due to sulfur loss from the cluster opens up the system to Mo-hydride formation, with H_2 then being formed via reaction with a sulfur-bound proton – either based on PTM-ligated sulfhydryl or H_2S.[45]

CONCLUSIONS

We find that a reactant-accessible, agglomeration-immune, polythiometalate – $CoMo_6S_{24}$@NU1K – can be obtained in quantitative yield by isolating the corresponding Anderson POM, in pore-size-matching fashion, within a hierarchically porous MOF and then heating the ensemble under flowing H_2S to exchange oxygen for sulfur. The resulting PTMs are unencumbered by capping ligands, but present a rich sulfur environment comprising S^{2-}, SH^-, and S_2^{2-}. With the majority of the cluster's sulfur ions accessible to candidate reactants, high catalytic, electrocatalytic, and/or photocatalytic activity for suitably chosen reactions might be expected. Indeed, when assembled as thin-films on electrodes, $CoMo_6S_{24}$@NU1K samples are competent for hydrogen evolution from aqueous acid. The films display kinetic overpotentials of just 100 mV at a benchmark current density of 10 mA/cm^2. The high activity accrues, at least in part, from the ability of the hybrid material to present the equivalent of *ca.* 500 monolayers of closed-packed PTM clusters, but in a mechanically, chemically, and thermally stable matrix featuring ample molecular-scale porosity.

Suspensions of $CoMo_6S_{24}$@NU1K crystallites, when irradiated at 390 nm, yield MOF linker excited-states that can readily reduce PTMs and thereby sensitize the reductive catalytic formation of H_2 from water. We find, however, that hydrogen evolution is preceded by a four-hour induction period during which the PTMs shed sulfurs and expose metal ions. The loss, which is limited to sulfur, translates to between 3.5 and 6 sulfur anions per PTM after 30 hours. Thus, at least for photochemical conversion of residual water to dihydrogen, the as-synthesized PTM is a pre-catalyst for the catalytically competent species, $CoMo_6S_{24-x}^{y-}$ @NU1K, where x is large enough to expose multiple cluster metal ions to reactive substrates. An attractive, albeit speculative, interpretation of the onset of catalytic activity with sulfur loss, is that the loss permits formation of Mo-hydride, which, in turn, can combine with sulfur-bound protons to form H_2. Notably, this mechanism, which is reminiscent of that used by hydrogenase, has been shown to be important for MOF-node-grafted, single-metal(molybdenum)-atom catalysts that feature, in the resting state, a pair of sulfhydryl ligands and a distorted tetrahedral coordination environment that leaves two sites open for substrate binding.[31] Further work will be required, however, to establish mechanisms.

Given the great variety of extant POMs and the large number of water-stable, extant Zr-MOFs,[46-49] we suggest that POM isolation and immobilization, based on pore-size matching, will provide synthetic access to a large and varied family of capping-ligand-free PTMs of well-defined metal-nuclearity and abundant catalytic activity for bond-forming reduction reactions. If the observed reduction-initiated loss of multiple sulfur anions from $CoMo_6S_{24}$@NU1K is more general phenomenon, then PTMs should be capable of presenting multiple open coordination sites (candidate reactant binding sites) on immediately proximal, redox-active metal-ions. Further, a PTM as simple as $CoMo_6S_{24-x}^{y-}$@NU1K should, in principle, be capable of mediating the delivery of a dozen or more electrons, based on Mo(IV/II) and Co(II/I/0) redox couples. The simultaneous presence of coordinated sulfide (weak base) and sulfhydryl (weak acid) species as PTM ligands could, in principle, usefully assist with proton management. While the MOF-immobilized PTM arrays described here are satisfyingly active for electrocatalytic and framework-sensitized photocatalytic hydrogen evolution, the real promise of these new clusters may be as metal-nuclearity-defined catalysts, electro-catalysts, and photo-catalysts for more complex reduction reactions.

ASSOCIATED CONTENT

Supporting Information

Experimental details, computational details and additional characterization (FTIR, DED, SEM, EDS mapping, dPDF, EXAFS fitting results, PXRD, XPS). This material is available free of charge via the Internet at http://pubs.acs.org.

AUTHOR INFORMATION

Corresponding Authors*

*qin0623@ustc.edu.cn,

*j-hupp@northwestern.edu

Notes

The authors declare no competing financial interest.

Author Contributions

J. Duan and H. Shabbir contributed equally to this work. The manuscript was written through the contributions of all authors. All authors have given approval for the final version of the manuscript.

ACKNOWLEDGMENTS

This work was initially supported as part of the Inorganometallic Catalyst Design Center, an EFRC funded by the DOE, Office of Science, Basic Energy Sciences (DE-SC0012702), and subsequently as part of the Catalyst Design for Decarbonization Center EFRC (DE-SC0023383), Electrocatalysis and photocatalysis studies were supported by the DOE, Office of Science, Basic Energy Sciences, Solar Photochemistry Program (grant DE-FG02-87ER13808 to J.T.H.) and Northwestern University. Q. L. thanks Wangsheng Chu for EXAFS fitting and Lei Feng for TOC drawing. Q. L. acknowledge the financial support from the National Natural Science Foundation of China (No. 11705205). W. B. acknowledge the financial support from the Natural Science Foundation of China (No. U1832168, 22175051), the Anhui Provincial Natural Science Foundation (No. 1808085MB26). Research in the Stupp laboratory (photocatalysis) was supported by the Center for Bio-Inspired Energy Science, an Energy Frontier Research Center funded by the U.S. Department of Energy, Office of Science, Basic Energy Sciences under Award No. DE-SC0000989. This work made use of the J.B. Cohen X-ray Diffraction Facility supported by the IMRSEC program of the National Science Foundation (DMR-1121262) at the Materials Research Center of Northwestern University. This work made use of the EPIC and Keck-II facilities of the NUANCE Center at Northwestern University, which has received support from the Soft and Hybrid Nanotechnology Experimental (SHyNE) Resource (NSF ECCS-1542205); the MRSEC program (NSF DMR-1720139) at the Materials Research Center; the International Institute for Nanotechnology (IIN); the Keck Foundation; and the State of Illinois, through the IIN. Use of the Advanced Photon Source is supported by the U.S. Department of Energy, Office of Science, and Office of Basic Energy Sciences, under Contract DE-AC02-06CH11357. Materials Research Collaborative Access Team (MRCAT, Sector 5-BM) operations are supported by the Department of Energy and the MRCAT member institutions.

ABBREVIATIONS

POM, polyoxometalate; poly*thio*metalates, PTMs; MOFs, metal-organic frameworks; NU, Northwestern University; $TBAPy^{4-}$, 1,3,6,8-tetrakis(p-benzoate)pyrene; FT-IR, Fourier transform-Infrared spectroscopy; ICP-OES, inductively coupled plasma optical emission spectroscopy; SEM-EDS, scanning electron microscopy energy dispersive X-ray spectroscopy; PXRD, powder X-ray diffraction; DED, difference envelop density; BET, Brunauer-Emmett-Teller; DRIFTS, diffuse reflectance infrared Fourier transform spectroscopy.

REFERENCES

(1) Kanady, S. J.; Lin, H. P.; Carsch, M. K.; Nielsen, J. R.; Takase, K. M.; Goddard, A.W.; III, Agapie, T. Toward Models for the Full Oxygen-Evolving Complex of Photosystem II by Ligand Coordination To Lower the Symmetry of the Mn_3CaO_4 Cubane: Demonstration That Electronic Effects Facilitate Binding of a Fifth Metal. *J. Am. Chem. Soc.* **2014,** *136,* 14373-14376.

(2) Mukherjee, S.; Stull, A. J.; Yano, J.; Stamatatos, C. T.; Pringouri, K.; Stich, A. T.; Abboud, A. K.; R. David Britt, Vittal K. Yachandra, George Christou. Synthetic model of the asymmetric $[Mn_3CaO_4]$ cubane core of the oxygen-evolving complex of photosystem II. *Proc. Natl. Acad. Sci.* **2012,** *109,* 2257-2262.

(3) Sankaralingam, M.; Lee, Y.; Galvan, Y.; Karmalkar, G. D.; Seo, S. M.; Jeon, S.; Pushkar, Y.; Fukuzumi, S.; Nam, W. Redox Reactivity of a Mononuclear Manganese-Oxo Complex Binding Calcium Ion and Other Redox-Inactive Metal Ions. *J. Am. Chem. Soc.* **2019,** *141,* 1324-1336.

(4) Ogo, S.; Kishima, T.; Yatabe, T.; Miyazawa, K.; Yamasaki, R.; Matsumoto, T.; Ando, T.; Kikkawa, M.; Isegawa, M.; Yoon, K.; Hayami, S. [NiFe], [FeFe], and [Fe] hydrogenase models from isomers. *Sci. Adv.* **2020,** *6,* 8181-8191.

(5) Britt, R. D.; Rao, G.; Tao, L. Bioassembly of complex iron-sulfur enzymes: hydrogenases and nitrogenases. *Nat. Rev. Chem.* 2**020,** *4,* 542-549.

(6) McSkimming, A.; Suess, L. M. D. Dinitrogen binding and activation at a molybdenum-iron-sulfur cluster. *Nat. Chem.* **2021,** *13,* 666-670.

(7) Zuo, J.; Zhou, H. C.; Holm, R. H. Vanadium-iron-sulfur clusters containing the cubane-type [VFe_3S_4] core unit: synthesis of a cluster with the topology of the PN cluster of nitrogenase. *Inorg. Chem.* **2003,** *42,* 4624-4631.

(8) Jordan, F. S.; Ioannou, I.; Rammu, H.; Halpern, A.; Bogart, K. L.; Ahn, M.; Vasiliadou, R.; Christodoulou, J.; Maréchal, A.; Lane, N. Spontaneous assembly of redox-active iron-sulfur clusters at low concentrations of cysteine. *Nat. Commun.* **2021,** *12,* 5925-5939.

(9) Henthorn, T. J.; Arias, J. R.; Koroidov, S.; Kroll, T.; Sokaras, D.; Bergmann, U.; Rees, C. D.; DeBeer, S. Localized Electronic Structure of Nitrogenase FeMoco Revealed by Selenium K-Edge High Resolution X-ray Absorption Spectroscopy. *J. Am. Chem. Soc.* **2019,** *141,* 13676-13688.

(10) Pope, M. Heteropoly and Isopoly Oxometalates, Springer-Verlag, Berlin, **1983.**

(11) Horn, M. R., Singh, A., Alomari, S., Goberna-Ferron, S., Benages-Vilau, R., Chodankar, N., Motta, N., Ostrikov, K., MacLeod, J., Sonar, P., Gomez-Romero, P., Dubal, D. Polyoxometalates (POMs): from electroactive clusters to energy materials. *Energy Environ. Sci.*, **2021,** *14*, 1652-1700.

(12) Alexander V. Anyushin, Aleksandar Kondinski, Tatjana N. Parac-Vogt, Hybrid polyoxometalates as post-functionalization platforms: from fundamentals to emerging applications. *Chem. Soc. Rev.* **2020,** *49,* 382-432.

(13) Gumerova, I. N.; Rompel, A. Synthesis, structures and applications of electron-rich polyoxometalates. *Nat. Rev. Chem.* **2018,** *2,* 0112.

(14) Wang, Q.; Xu, B.; Wang, Y.; Wang, H.; Hu, X.; Ma, P.; Niu, J.; Wang, J. Polyoxometalate-Incorporated Framework as a Heterogeneous Catalyst for Selective Oxidation of C-H Bonds of Alkylbenzenes. *Inorg. Chem.* **2021,** *60,* 7753-7761.

(15) Mercè Martin-Sabi, Joaquín Soriano-López, Ross S. Winter, Jia-Jia Chen, Laia Vilà-Nadal, De-Liang Long, José Ramón Galán-Mascarós & Leroy Cronin. Redox tuning the Weakley-type polyoxometalate archetype for the oxygen evolution reaction. *Nat. Catal.* **2018,** *1,* 208-213.

(16) Cui, J. W.; Zhang, M. S.; Ma, Y. Y.; Wang, Y.; Miao, X. R.; Han, G. Z. Polyoxometalate-Incorporated Metal-Organic Network as a Heterogeneous Catalyst for Selective Oxidation of Aryl Alkenes. *Inorg. Chem.* **2022,** *61,* 9421–9432.

(17) Liu, Q.; Chen, Z.; Shabbir, H.; Duan, J.; Bi, W.; Lu, Z.; Schweitzer, M. N.; Alayoglu, S.; Goswami, S.; Chapman, K.; Getman, B. R.; Wang, Q.; Notestein, M. J.; Hupp, T. J. Presentation of gas-phase-reactant-accessible single rhodium-atom catalysts for CO oxidation, *via* MOF confinement of an Anderson polyoxometalate. *J. Mater. Chem. A* **2022,** *10,* 18226-18234.

(18) Buru, T. C.; Li, P.; Mehdi, L. B.; Dohnalkova, A.; Prats, E. P. A.; Browning, D. N.; Chapman, W. K.; Hupp, T. J.; Farha, K. O. Adsorption of a Catalytically Accessible Polyoxometalate in a Mesoporous Channel-type Metal-Organic Framework *Chem. Mater.* **2017,** *29,* 5174-5181.

(19) Buru, T. C.; Wasson, C. M.; Farha, K. O. $H_5PV_2Mo_{10}O_{40}$ Polyoxometalate Encapsulated in NU-1000 Metal-Organic Framework for Aerobic Oxidation of a Mustard Gas Simulant. *ACS Appl. Nano Mater.* **2020,** *3,* 658-664.

(20) Mondloch, E. J.; Bury, W.; Jimenez, F. D.; Kwon, S.; DeMarco, J. E.; Weston, H. M.; Sarjeant, A. A.; Nguyen, T. S.; Stair, C. P.; Snurr, Q. R.; Farha, K. O.; Hupp, T. J. Vapor-Phase Metalation by Atomic Layer Deposition in a Metal-Organic Framework. *J. Am. Chem. Soc.* **2013,** *135,* 10294-10297.

(21) Zhou, H. C.; Long, J. R.; Yaghi, O. M. Introduction to Metal-Organic Frameworks. *Chem. Rev.* **2012,** *112,* 673-674.

(22) Bai, Y.; Dou, Y.; Xie, L.; Rutledge, W.; Li, J.; Zhou, H.; Zr-based metal-organic frameworks: design, synthesis, structure, and applications. *Chem. Soc. Rev.* **2016,** *45,* 2327-2367.

(23) Stylianou, C. K.; Heck, R.; Chong, Y. S.; Bacsa, J.; Jones, T. A. J.; Khimyak, Z. Y.; Bradshaw, D.; Rosseinsky, J. M. A Guest-Responsive Fluorescent 3D Microporous Metal-Organic Framework Derived from a Long-Lifetime Pyrene Core. *J. Am. Chem. Soc.* **2010,** *132,* 4119-4130.

(24) Yang, D.; Gates, C. B. Elucidating and Tuning Catalytic Sites on Zirconium- and Aluminum-Containing Nodes of Stable Metal-Organic Frameworks. *Acc. Chem. Res.* **2021,** *54*, 1982–1991

(25) Lu, Z.; Liu, J.; Zhang, X.; Liao, Y.; Wang, R.; Zhang, K.; Lyu, J.; Farha, K. O.; Hupp, T. J. Node-Accessible Zirconium MOFs. *J. Am. Chem. Soc.* **2020,** *142,* 50, 21110-21121.

(26) Webber, E. T.; Liu, G. W.; Desai, P. S.; Lu, C. C.; Truhlar, G. D.; Penn, L. R. Role of a Modulator in the Synthesis of Phase-Pure NU-1000. *ACS Appl. Mater. Interfaces* **2017,** *9,* 39342-39346.

(27) Blazevic, A.; Rompel, A. The Anderson-Evans polyoxometalate: From inorganic building blocks via hybrid organic-inorganic structures to tomorrows "Bio-POM" *Coord. Chem. Rev.* **2016,** *307,* 42-64.

(28) Liu, Q.; Li, X.; He, Q.; Khalil, A.; Liu, D.; Xiang, T.; Wu, X.; Song, L. Gram-Scale Aqueous Synthesis of Stable Few-Layered 1TMoS_2: Applications for Visible-Light-Driven Photocatalytic Hydrogen Evolution. *Small* **2015,** *11,* 5556-5564.

(29) Huang, Y.; Sun, Y.; Zheng, X.; Aoki, T.; Pattengale, B.; Huang, J.; He, X.; Bian, W.; Younan, S.; Williams, N.; Hu, J.; Ge, J.; Pu, N.; Yan, X.; Pan, X.; Zhang, L.; Wei, Y.; Gu, J. Atomically engineering activation sites onto metallic 1T-MoS_2 catalysts for enhanced electrochemical hydrogen evolution. *Nat. Commun.* **2019,** *10,* 1-11.

(30) Hod, I.; Deria, P.; Bury, W.; Mondloch, J. E.; Kung, C. W.; So, M.; Sampson, M. D.; Peters, A. W.; Kubiak, C. P.; Farha, O. K.; Hupp, J. T. A Porous Proton-Relaying Metal-Organic Framework Material that Accelerates Electrochemical Hydrogen Evolution. *Nat. Commun.* **2015,** *6,* 8304.

(31) Noh, H.; Kung, C.; Otake, K.; Peters, W. A.; Li, Z.; Liao, Y.; Gong, X.; Farha, K.O.; Hupp, T. J. Redox-Mediator-Assisted Electrocatalytic Hydrogen Evolution from Water by a

Molybdenum Sulfide-Functionalized Metal-Organic Framework. *ACS Catal.* 2**018,** *8,* 9848-9858.

(32) Yakovenko, Andrey A.; Wei, Z.; Wriedt, M.; Li, J.-R.; Halder, J. G.; Zhou, H.-C. Study of Guest Molecules in Metal–Organic Frameworks by Powder X-ray Diffraction: Analysis of Difference Envelope Density. *Cryst. Growth Des.* **2014,** *14,* 5397-5407.

(33) Platero-Prats, A. E.; League, A. B.; Bernales, V.; Ye, J.; Gallington, L. C.; Vjunov, A.; Schweitzer, N. M.; Li, Z.; Zheng, J.; Mehdi, B. L.; Stevens, A. J.; Dohnalkova, A.; Balasubramanian, M.; Farha, O. K.; Hupp, J. T.; Browning, N. D.; Fulton, J. L.; Camaioni, D. M.; Lercher, J. A.; Truhlar, D. G.; Gagliardi, L.; Cramer, C. J.; Chapman, K. W. Bridging Zirconia Nodes within a Metal-Organic Framework via Catalytic Ni-Hydroxo Clusters to Form Heterobimetallic Nanowires. *J. Am. Chem. Soc.* **2017**, *139*, 10410-10418.

(34) Klet, C. R.; Liu, Y.; Wang, C. T.; Hupp, T. J.; Farha, K. O. Evaluation of Brønsted acidity and proton topology in Zr- and Hf-based metal–organic frameworks using potentiometric acid–base titration. *J. Mater. Chem. A* **2016,** *4,* 1479-1485.

(35) Hou, J.; Zhang, B.; Li, Z.; Cao, S.; Sun, Y.; Wu, Y.; Gao, Z.; Sun, L. Vertically Aligned Oxygenated-CoS_2-MoS_2 Heteronanosheet Architecture from Polyoxometalate for Efficient and Stable Overall Water Splitting. *ACS Catal.* **2018,** *8,* 4612-4621.

(36) Deng, J.; Li, H.; Xiao, J.; Tu, Y.; Deng, D.; Yang, H.; Tian, H.; Li, J.; Ren P.; Bao, X. Triggering the electrocatalytic hydrogen evolution activity of the inert two-dimensional MoS_2 surface via single-atom metal doping. *Energy Environ. Sci.,* **2015,** *8,* 1594.

(37) Wang, H.; Tsai, C.; Kong, D.; Chan, K.; Pedersen, A. F.; Nørskov, K. J.; Cui, Y. Transition-metal doped edge sites in vertically aligned MoS_2 catalysts for enhanced hydrogen evolution. *Nano Res.* **2015,** *8,* 566-575.

(38) Park, S.; Park, J.; Abroshan, H.; Zhang, L.; Kim, K. J.; Zhang, J.; Guo, J.; Siahrostami, S.; Zheng, X. Enhancing Catalytic Activity of MoS_2 Basal Plane S-Vacancy by Co Cluster Addition. *ACS Energy Lett.* **2018,** *3,* 2685-2693.

(39) Shi, Y.; Zhou, Y.; Yang, R. D.; Xu, W. X.; Wang, C.; Wang, F. B.; Xu, J. J.; Xia, X. H.; Chen, Y. H. Energy Level Engineering of MoS_2 by Transition-Metal Doping for Accelerating Hydrogen Evolution Reaction. *J. Am. Chem. Soc.* **2017,** *139,* 15479-15485.

(40) Dai, X.; Liu, M.; Li, Z.; Jin, A.; Ma, Y.; Huang, X.; Sun, H.; Wang, H.; Zhang, X. Molybdenum Polysulfide Anchored on Porous Zr-Metal Organic Framework to Enhance the Performance of Hydrogen Evolution Reaction. *J. Phys. Chem. C* **2016,** *120,* 12539-12548.

(41) Shinagawa, T.; Garcia-Esparza, T. A.; Takanabe, K. Insight on Tafel slopes from a microkinetic analysis of aqueous electrocatalysis for energy conversion. *Sci. Rep.* **2015,** *5,* 13801.

(42) Zhang, K.; Goswami, S.; Noh, H.; Lu, Z.; Sheridan, T.; Duan, J.; Dong, Wei.; Hupp. T. J. An iron-porphyrin grafted metal-organic framework as a heterogeneous catalyst for the photochemical reduction of CO_2. *J. Photochem. Photobiol* **2022,** *10,* 100111-1001118.

(43) Goswami, S.; Yu, J.; Patwardhan, S.; Deria, P.; Hupp, T. J. Light-Harvesting "Antenna" Behavior in NU-1000. *ACS Energy Lett.* **2021,** *6,* 848–853.

(44) Li, H.; Tsai, C.; Koh, L. A.; Cai, L.; Contryman, W. A.; Fragapane, H. A.; Zhao, J.; Han, S. H.; Manoharan, C. H.; A-Pedersen, F.; Nørskov, K. J.; Zheng, X. Activating and optimizing MoS_2 basal planes for hydrogen evolution through the formation of strained sulphur vacancies. *Nat. Mater.* **2016,** *15,* 48-53.

(45) Bau, A. J.; Emwas, -H. A.; Nikolaienko, P.; Aljarb, A. A.; Tung, V.; Rueping, M. Mo^{3+} hydride as the common origin of H_2 evolution and selective NADH regeneration in molybdenum sulfide electrocatalysts. *Nat. Catal.* **2022,** *5,* 397-404.

(46) Øien-Ødegaard, S.; Shearer, C. G.; Wragg, S. D.; Lillerud, P. K. Pitfalls in metal–organic framework crystallography: towards more accurate crystal structures**.** *Chem. Soc. Rev.* **2017,** *46,* 4867-4876

(47) Y. Zhang, J. Phipps, S. Ma. Artificial enzymes for artificial photosynthesis. *Nat. Catal.* **2022,** *5,* 973-974.

(48) Nguyen, D. K.; Ehrling, S.; Senkovska, I.; Bon, V.; Kaskel, S. New 1D chiral Zr-MOFs based on in situ imine linker formation as catalysts for asymmetric CC coupling reactions. *J. Catal.* **2020,** *386,* 106-116.

(49) Kalaj, M.; Bentz, C. K.; Jr, A. S.; Palomba, M. J.; Barcus, S. K.; Katayama, Y.; Cohen, M. S. MOF-polymer hybrid materials: from simple composites to tailored architectures. *Chem. Rev.* **2020,** *120,* 8267-8302.

For Table of Contents Only

Isolated $CoMo_6S_{24}$ clusters were encapsulated within a hierarchically porous MOF NU1K and catalytically active for an illustrative hydrogen evolution reaction.